Geosci. Model Dev. Discuss., doi:10.5194/gmd-2016-110, 2016
Manuscript under review for journal Geosci. Model Dev.
Published: 1 August 2016

Geoscientific Model Development Discussions
Open Access
EGU

Development of a new gas flaring emission data set for southern West Africa

Konrad Deetz, Bernhard Vogel

Karlsruhe Institute of Technology (KIT), Institute of Meteorology and Climate Research – Troposphere Research (IMK-TRO), Hermann-von-Helmholtz 1, 76344 Eggenstein-Leopoldshafen

HIGHLIGHTS

- Development of a new gas flaring emission parameterization for air pollution modeling.
- Combination of remote sensing observation and physical based combustion calculation.
- Application to the significant gas flaring region southern West Africa.
- Comprehensive assessing of the parameterization uncertainties.
- Comparison with existing gas flaring emission inventories.

Keywords:

Gas flaring
Emission parameterization
Emission uncertainty
Pollution modeling
Carbon dioxide

ABSTRACT

A new gas flaring emission parameterization has been developed which combines remote sensing observations using VIIRS nighttime data with combustion equations. The parameterization has been applied to southern West Africa, including the Niger Delta as a region which is highly exposed to gas flaring. Two two-month datasets for June-July 2014 and 2015 were created. The parameterization delivers emissions of CO, CO_2, NO and NO_2. A flaring climatology for both time periods has been derived. The uncertainties owing to cloud cover, parameter selection, natural gas composition and the interannual differences are assessed. Largest uncertainties in the emission estimation are linked to the parameter selection. By using remote sensing cloud cover observations, a correction factor for the climatology was established to consider the effect of flares masked by clouds. It can be shown that the flaring emissions in SWA have significantly decreased by 30% from 2014 to 2015. Existing emission inventories were used for validation. CO_2 emissions with the estimated uncertainty in brackets of 8 $(^{12}/_{2})$ Tg y^{-1} for 2014 and 5 $(^{7}/_{1})$ Tg y^{-1} for 2015 are derived. The flaring emission estimation within this study for June-July 2014 is in the same order of magnitude compared to existing emission inventories. For the same period in 2015 the emission estimation is one order of magnitude smaller in comparison to existing inventories. The deviations might be attributed to uncertainties in the derived flare gas flow rate, the decreasing trend in gas flaring or inconsistent emission sector definitions. The parameterization source code is available as a package of R scripts.

1. Introduction

Gas flaring is a globally used method to dispose flammable, toxic or corrosive vapors to less reactive compounds at oil production sites and refineries. In regions of insufficient transportation infrastructure or missing consumers, flaring is also commonly applied.

CDIAC (2015a) estimated the global gas flaring emission of carbon dioxide to 267.7 million tons (0.83% of total emissions) in 2008. Flaring and venting of gas significantly contributes to the greenhouse gas emissions and therefore to the global climate change. The five countries with the highest flaring amount in billion cubic meter (bcm) are Russia (35), Nigeria (15), Iran (10), Iraq (10) and USA (5) (World Bank, 2012).

In recent time, especially with the development of remote sensing observation techniques (e.g. Elvidge et al. (1997, 2013)), emissions from gas flaring moved in the focus of atmospheric research involving the efforts in reducing the pollution and the waste of resources. The World Bank led the initiatives “Global Gas Flaring Reduction Partnership” (GGFR) and “Zero Routine Flaring by 2030” to promote the efficient use of flare gas.

Instead of relying on national statistics of gas production and consumption for estimating the flaring amount, remote sensing techniques can estimate the flaring amount directly via multispectral data (Elvidge et al., 2013). Elvidge et al. (2009) developed a 15 year dataset of global and national gas flaring efficiency from 1994 to 2008 by using data from the Defense Meteorological Satellite Program (DMSP). Doumbia et al. (2014) combined DMSP with emission factors for flaring, to estimate the flaring emissions for SWA. The satellite product Visible Infrared Imaging Radiometer Suite (VIIRS) Nightfire (Elvidge et al., 2013), which is free available as “VIIRS Nightfire Prerun V2.1 Flares only” (VIIRS, 2015) (VNP hereafter), is now the most widely used product to derive flaring emissions from satellite imagery. By using VNP, Zhang et al. (2015) estimated the methane consumption and the release of CO_2 from gas flaring for the northern U.S. which agree with field data within an uncertainty range of $\pm$50%.

Also in the second largest flaring country Nigeria, the awareness of gas flaring increases. On gasflaretracker.ng the attention of the government, industry and society is called to the flaring problem by interactive maps of flare infrastructure, amounts and costs. The implications of gas flaring in Nigeria are far-reaching. It influences the environment by noise and deterioration of the air quality (Osuji and Avwiri, 2005). Nwankwo and Ogagarue (2011) have measured higher concentrations of heavy metals in surface water of a gas flared environment in Delta State Nigeria. Adverse ecolological and bacterial spectrum modifications by gas flaring are indicated by Nwaugo et al. (2006). Gas flaring also causes acid rain which causes economic burden via rapid corrosion of zinc roofs (Ekpoh and Obia, 2010) and causes retardation in crop growth owing to high temperatures (Dung et al., 2008).

The project DACCIWA (Dynamics-aerosol-cloud interactions in West Africa, Knippertz et al. (2015)) investigates the influence of anthropogenic and natural emissions on the atmospheric composition over SWA, including the flaring hotspot Nigeria, to examine the meteorological and socio-economic effects. To consider the SWA gas flaring emissions (e.g. in an atmospheric model), this study presents a method to derive emission fluxes by combining the state of the art flaring detection VNP and the combustion equations of Ismail and Umukoro (2014) which does not use emission factors. The new parameterization is robust and easy to apply to new research questions according flexibility in the spatiotemporal resolution.

The parameterization is presented in Section 2. Results of the application to SWA, including the spatial distribution of gas flaring, the emission estimation and the uncertainty assessment are investigated in Section 3. Section 4 places the emission estimates in the context of existing inventories. The results are summarized and discussed in Section 5.

2. Parameterization of gas flaring emissions

Geosci. Model Dev. Discuss., doi:10.5194/gmd-2016-110, 2016
Manuscript under review for journal Geosci. Model Dev.
Published: 1 August 2016

Geoscientific Model Development Discussions

The new parameterization for gas flaring presented here, is based on VNP (VIIRS Nightfire Prerun V2.1 Flares only) and the combustion equations of Ismail and Umukoro (2014) (IU14 hereafter).

2.1 Remote sensing identification of gas flares

VIIRS (Visible Infrared Imaging Radiometer Suite) is a scanning radiometer for visible and infrared light on board the sun-synchronous Suomi National Polar-orbiting Partnership weather satellite (Suomi-NPP) (NASA, 2016). It can detect combustion sources at night (e.g. bush fires or gas flares) by spectral band M10. To confirm these sources and to eliminate noise, the Day/Night Band (DNB), M7, M8 and M12 are used in addition. By fitting these measured spectra to the Planck radiation curve, background and source temperatures can be deduced. VNP is filtered to include only detections with temperatures between 1600 K and 2000 K, which is believed to be an adequate estimation for average gas flares. Up to now no atmospheric correction is done (VIIRS, 2015).
The data is freely available as daily data from March 2014 to present. The files include among others the location of the flares, source temperature T_s, radiant heat H and time of observation.
For this study we have decided for a two month period of observation. This allows a compilation of a flaring climatology in terms of the locations and emissions and a robust estimation of uncertainty owing to cloud coverage and other parameters that have to be prescribed for IU14. We have selected the month June and July because the gas flaring emission dataset will be used within the regional online-coupled chemistry model COSMO-ART (Vogel et al., 2009) during the measurement campaignof the project DACCIWA, which takes place in June/July 2016. This campaign includes airborne, ground based and remote sensing observations of meteorological conditions and air pollution characteristics. COSMO-ART is one of the forecasting models of the DACCIWA campaign and delivers spatiotemporal aerosol/chemistry distributions. The data for 2014 and 2015 are used to allow also for an interannual comparison, to assess the uncertainty owing to changes in flare processes (e.g. built-up or dismantling, increase or decrease in combustion).
For this study we use location, source temperature and radiant heat for days with sufficient satellite coverage over the research domain SWA with a focus on the Niger Delta.

2.2 Emission estimation method

The principle emission estimation methodology used in this study follows IU14. The gas flaring emissions are estimated based on combustion equations for incomplete combustion including six flaring conditions given in Tab. 1. The equations are introduced in detail in IU14 and are therefore not presented here. This section concentrates on the application of the method of IU14 to the VNP data and the research domain in SWA.

Tab.1. Reaction types for incomplete combustion of flared gas, depending on availability of sulfur in the flared gas and the temperature in the combustion zone which determines the formation of NO and NO_2.

Reaction type	Sulfur in flared gas	Source temperature (K)	NO_x formation
1	No	< 1200	no
2	Yes	< 1200	no
3	No	$1200 \leq T_s \leq 1600$	only NO
4	Yes	$1200 \leq T_s \leq 1600$	only NO
5	No	> 1600	NO and NO_2
6	Yes	> 1600	NO and NO_2

Geosci. Model Dev. Discuss., doi:10.5194/gmd-2016-110, 2016
Manuscript under review for journal Geosci. Model Dev.
Published: 1 August 2016

As input, IU14 needs the natural gas composition C of the fuel input of the flare, the source temperature T_s (temperature in the combustion zone), and the flare characteristics including combustion efficiency η (1 is complete combustion without Carbon monoxide formation) and availability of combustion air δ (above 1 is excess and below 1 is deficiency). In addition we need the flow rate F, the gauge pressure of the fuel gas in the flare p_g, and the fraction of total reaction energy that is radiated f. The value for f is estimated by averaging a table of literature values for f given in Guigard et al. (2000). The IU14 input is summarized in Tab. 2.

Tab.2. Variables and parameters needed for IU14 or for deriving the fluxes of the air pollutants

Parameter	Description	Reference	Unit
C	Natural gas composition	Sonibare and Akeredolu (2004)	%
T_s	Source temperature	VNP (VIIRS, 2015)	K
η	Combustion efficiency	0.8 (IU14)	-
δ	Availability of combustion air	0.95 (IU14)	-
H	Radiant heat	VNP (VIIRS, 2015)	MW
F	Flow rate	VNP (VIIRS, 2015), TA-Luft (1986)	$m^3 s^{-1}$
p_g	Gauge pressure	34.475 (API, 2007)	kPa
f	Fraction of radiated heat	0.27 (Guigard et al., 2000)	-

The natural gas composition is taken from Sonibare and Akeredolu (2004). They have measured the molar composition of Nigerian natural gas in the Niger Delta area for ten gas flow stations. For this study we have calculated the average over these stations and merged the data according their number of carbon atoms (Tab. 3). H_2S fraction is rather low because it was detected only in two out of the ten flow stations.

Tab.3. Molar composition of natural gas in Niger Delta (Nigeria) based on the measurements of Sonibare and Akeredolu (2004), averaged over ten flow station. The hydrocarbons are merged according to the number of C atoms.

Constituent	Fraction (%)
Methan (CH_4)	78.47
Ethan (C_2H_6)	6.16
Propane (C_3H_8)	5.50
Butan (C_4H_{10})	5.19
Pentane (C_5H_{12})	3.95
Hexane (C_6H_{14})	0.36
Carbon dioxide (CO_2)	0.305
Nitrogen (N_2)	0.06
Hydrogen sulfide (H_2S)	0.005

The source Temperature T_s is taken from VNP. The combustion efficiency η was set to 0.8 and the availability of combustion air δ to 0.95. IU14 remarked, that the reaction condition for flaring of $\eta \gg 0.5$ and $\delta \geq 0.9$ should be the norm in regions, where the effective utilization of this gas is not available or not economically. Strosher (2000) indicate a combustion efficiency of solution gas at oil-field battery sites between 0.62 and 0.82, and 0.96 for flaring of natural gas in the open atmosphere under turbulent conditions. EPA (1985) shows combustion efficiencies between 0.982 and 1 for measurements on a flare screening facility. Section 3.3.2 will shed light on the uncertainty which arises from η and δ via a parameter sensitivity study. The authors strongly recommend a careful selection of η and δ since unrealistic combinations (e.g. higher combustion efficiencies with rather low availability of combustion air) can lead to negative NO and NO_2 emissions.

Geosci. Model Dev. Discuss., doi:10.5194/gmd-2016-110, 2016
Manuscript under review for journal Geosci. Model Dev.
Published: 1 August 2016

Geoscientific Model Development Discussions

The flow rate, gauge pressure and fraction of radiated heat are not included in the parameterization of IU14 but are necessary to derive the mass emission rates which can be used as emission data for an atmospheric dispersion model.

The flow rate F ($m^3\ s^{-1}$) is estimated by Eq. 1 (TA-Luft, 1986)

$$F = M/\left(1.36 \cdot 10^{-3}\,(T_S - 283)\right), \quad (1)$$

where M is the heat flow in MW and T_S the source temperature in K. We assume that the emitted heat flow M is equal to the total reaction energy of the flare. VNP only detects the energy fraction that is radiated H and not the total energy M. By using the radiant heat H (observed by VNP) and the factor f (fraction of H to the total reaction energy, Guigard et al., 2000), we estimate M as $H \cdot 1/f$. For the source temperature T_S we use the VNP observation.

The estimation of the fuel gas density, which is necessary to transform the flow rate F into an emission, is problematic due to the lack of data concerning the technical setup of the SWA flares. We assume that the dominating flare type is a low-pressure single point flare. Bader et al. (2011) pointed out that these flares are the most common flare type for onshore facilities that operate at low pressure (below 10 psi (69 kPa) above ambient pressure) and API (2007) remarks that most subsonic-flare seal drums operate in the range from 0 psi to 5 psi (34 kPa). Therefore we have decided for a gauge pressure p_g of 5 psi (34 kPa) above ambient pressure. Via Eq. 2 we can calculate the fuel gas density ρ_f

$$\rho_f = p_f/\left(R/(M_f\,T_a)\right), \quad (2)$$

where p_f is the fuel gas pressure as the sum of ambient pressure (10.1325 kPa, taken as const) and gauge pressure p_g. R is the universal gas constant, M_f the molar mass of the fuel gas and T_a the ambient temperature (293.15 K, taken as const). Finally, the emission E ($kg\ s^{-1}$) of a species i is given by

$$E_i = \frac{m_i}{m_{total}}\,\rho_f\,F, \quad (3)$$

where m_i is the mass of the species i and m_{total} the total mass of the fuel gas, both delivered by the parameterization of IU14.

The combustion calculations within IU14 provide the species water, hydrogen, oxygen, nitrogen, carbon dioxide, carbon monoxide, sulfur dioxide, nitrogen oxide and nitrogen dioxide. In the following only CO, SO_2, NO and NO_2 are considered. However, no black carbon or volatile organic compounds (VOCs) are considered by IU14, although they are not negligible. Johnson et al. (2011) estimated the mean black carbon emission for a large-scale flare at a gas plant in Uzbekistan to be 7400 g h^{-1} and Stroshers (1996) measured the concentration of predominant VOCs 5 m above the gas flare in Alberta with 458.6 mg m^{-3}. However, owing to the missing representation of black carbon and VOCs in IU14, these compounds are not considered in this study.

A flaring emission comparison between several days or averaging over a certain period is problematic due to small variances in the VNP locations of the flares. This means even the same flare can be detected on a slightly different position the next day, which makes an emission averaging for every single flare difficult, especially in intensive flare areas. We bypass the problem by predefining a grid and allocating the flares to this grid. By using the source code written in R (R Core Team, 2013) delivered by this study, the user can define the grid size independently. For calculating the average over several days, the emissions for every single flare per day are calculated and summed up according to their belonging to a certain grid box. This leads to one big point source per grid box. The corresponding emissions are then averaged over the time period of interest for every grid box (flare box herafter). Considering this approach within an atmospheric model, by selecting the same grid configuration for the flaring emission data and the model, no loss of information occurs.

3. Results

3.1 Spatial distribution of gas flaring in SWA

We have selected the two time periods June/July 2014 (TP14) and June/July 2015 (TP15) and omitted all days without observations or with insufficient data coverage for VNP over SWA. This leads to 58 (48) observations for TP14 (TP15).

In the preparation of this work we have compared the estimated mean locations of the flares of TP14 with the Google Earth imagery (Google Earth, 2014) (not shown). Only the onshore flares are visible in Google Earth. This visual verification reveals that 72% of the VNP detected onshore flares are visible in Google Earth. It is very likely that the hit rate is much higher since it is often the case that the Google Earth image quality is not good enough for verification or the images are not up to date. This comparison indicates that VNP is a valid method to identify the flares in SWA.

For the following analysis we have calculated the emissions for both time periods on a grid with a mesh size of 0.25° (28 km) from 10°S to 10°N and from 10°W to 15°E. Fig. 1 emphasizes the areas in which VNP detects flares only in TP14 (TP15) in red (green) color and in grey the areas with flaring in both periods.

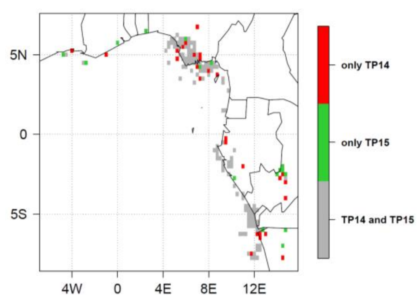

Fig.1. Flaring area for TP14 and TP15. Red (green) boxes denote areas with flaring only for TP14 (TP15). For the grey areas, flaring is detected in both time periods.

Remarkable are the dominating flaring areas in the Niger Delta and the adjacent offshore regions in the Gulf of Guinea. Also in the coastal region of Gabon, Republic of the Congo, Angola and sporadically along the coast of Ivory Coast, Ghana and Benin, flaring occurs. By comparing TP14 and TP15 more red than green areas are visible, especially in southern Nigeria, which indicates a reduction in the flaring area from 2014 to 2015. A decrease in CO_2 from 1994 to 2010, particularly in the onshore platforms is indicated by Doumbia et al. (2014).

The mean active flare density, as the sum over all detected flares in a box averaged over the time period, is shown in Fig. 2 for (a) TP14 and (b) TP15.

Geosci. Model Dev. Discuss., doi:10.5194/gmd-2016-110, 2016
Manuscript under review for journal Geosci. Model Dev.
Published: 1 August 2016

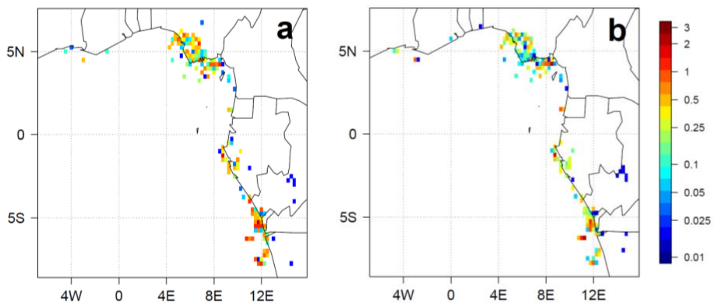

Fig.2. Mean active flare density (number of active flares per box) averaged over (a) TP14 and (b) TP15 in logarithmic scale

Fig. 2 shows to a a reduction in the active flare density in TP15 compared to TP14. 72% of the flaring area which TP14 and TP15 have in common, shows a reduction in TP15 about 48% on average. 28% of the common flaring area shows an increase in TP15 about 124%. Therefore it seems that the flaring intensity decreases in TP15 over large areas but simultaneously some flaring hotspots occurred, which are distributed along the SWA coast (not shown). Fig. 2, together with the variation of flaring emissions from TP14 to TP15 in Section 3.3.3, indicates the high year to year variations. This makes the use of past averaged conditions questionable, especially when certain episodes are studied.

3.2 Emission estimation

For the emission estimation we have used a climatological approach (E_{clim}). For every day with valid data in TP14 and TP15 the emissions for all detected flares are calculated separately and allocated to the predefined grid. The emissions are summed up in every flare box to have one joined flare per grid box. Finally the temporal average for every grid box is calculated over TP14 and TP15 respectively. Therefore all flares, detected in the time period, are active at once with their mean emission strength. This method has the advantage that most likely all flares in the domain are captured even if a fraction of them is covered by clouds at certain days. However, this could lead to an emission overestimation because not all available flares are active at once. This problem of separating between flares which are not active and flares which are active but covered by clouds and therefore not visible for VNP is picked up again in Section 3.3.1. Fig. 3 shows the emissions of CO, SO_2, NO and NO_2 in t h^{-1} for TP15.

Geosci. Model Dev. Discuss., doi:10.5194/gmd-2016-110, 2016
Manuscript under review for journal Geosci. Model Dev.
Published: 1 August 2016

Geoscientific Model Development Discussions
Open Access
EGU

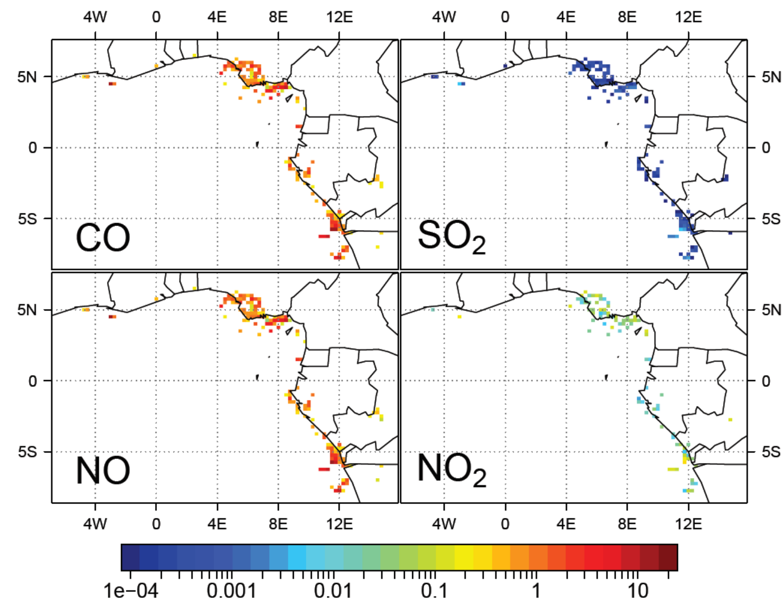

Fig.3. Flaring emissions for TP15 within E_{clim} in t h^{-1} for CO, SO_2, NO and NO_2

Highest emissions are calculated for carbon monoxide, followed by nitrogen oxide and nitrogen dioxide. Sulfur dioxide shows lowest emissions since these emissions do not depend on combustion processes but only on the natural gas composition (see Tab. 3) and the amount of flared gas (IU14). Due to the use of the averaged measurements of Sonibare and Akeredolu (2004), local variations of hydrogen sulfide concentrations in the natural gas cannot be taken into account. Hydrogen sulfide is the only source of sulfur in the flared gas and therefore determines the emission of sulfur dioxide. To assess this uncertainty, a sensitivity study with different hydrogen sulfide concentrations is given in Section 3.3.5.

3.3 Estimation of uncertainties

In the following section the most relevant uncertainties are presented, together with approaches for their assessment. This includes the uncertainty concerning the flare detection in the presence of cloud cover, the uncertainty in the determination of the emitted heat flow H via the fraction of radiated heat f, the uncertainty in the choice of the IU14 parameters and the changes in flare operation from one year to another as well as the influence of the spatial variability of hydrogen sulfide in the natural gas on the sulfur dioxide emissions. Apart from Section 3.3.4 all uncertainty estimations are confined to TP15.

3.3.1 Uncertainty due to cloud cover

In Section 3.2 a climatological data set of flaring emissions (E_{clim}) was derived. When using this data set we are losing the day to day variation of the flaring emissions that is delivered by VNP. Although daily satellite observations are available, the problem arises that usually parts of the scene observed by the satellite are covered by clouds. In the following we will describe a method of how to derive

Geosci. Model Dev. Discuss., doi:10.5194/gmd-2016-110, 2016
Manuscript under review for journal Geosci. Model Dev.
Published: 1 August 2016

daily flaring emissions based on the climatological emissions (E_{clim}), a threshold of cloud coverage (N_{th}), and the actual detected flares at a certain day. This is illustrated schematically by Fig. 4.

The closed grey pie in the lower layer of Fig. 4A gives the climatological number of flaring boxes in the research domain. At a certain day only within the green flaring boxes active flares are detected by VNP. The flaring boxes that are indicated in grey are those at which no active flares were detected by VNP, either because they are inactive or obscured by clouds. We now further separate this grey area by introducing an empirical threshold value N_{th} of cloud cover. In areas that belong to the grey fraction in Fig 4A, where the cloud cover is above N_{th}, we assume that the flares boxes are active and emit with their climatological emission values (since there are no current observations available). Those flare boxes are indicated by the dark blue color in Fig 4B. The light blue area indicates flare boxes where the cloud cover is below N_{th} and where no flares are detected by VNP. For this area we postulate that all flare boxes are inactive and consequently have zero emissions. Finally we calculate the total emissions at a certain day for N_{th}=50% (E_{50}), 75% (E_{75}) and 90% (E_{90}) as the sum of the climatological emissions in the dark blue area and the directly detected flares in the green area.

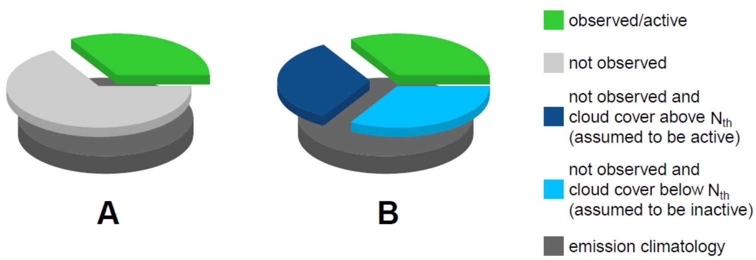

Fig.4. Pie charts illustrating the flaring emission uncertainty assessment due to cloud cover for TP15. The entirety of the flare boxes within the emission climatology (E_{clim}) is given as closed grey pie in the bottom of **A** and **B**. **A** distinguishes between flare boxes in which flares are detected at a certain day (green) and the complement of undetected flare boxes (light grey). In **B** the light grey slice of **A** is separated in a cloud-covered (above cloud cover threshold N_{th}, dark blue) and cloud-free (below N_{th}, light blue) by using remote sensing observations. Flare boxes which are not detected by VNP and simultaneously show a cloud cover above N_{th}, are taken as active. Flare boxes which are not detected by VNP and simultaneously show a cloud cover below N_{th}, are taken as inactive. For N_{th} the values 50%, 75% and 90% are used. The higher N_{th} the smaller the dark blue slice in **B**.

To separate the light grey slice in Fig. 4A in covered and uncovered flare boxes, we used instantaneous cloud fractional cover (CFC) from the geostationary Meteosat Second Generation 3 (MSG3) (CM SAF, 2015, copyright (2015) EUMETSAT) for every day of TP15 around the time of VNP observation (Suomi-NPP overflight approx. at 1 UTC). This method is applied to all days of TP15 for every flare box.

To ensure a consistent timing between cloud observation and VNP observation, the spatial domain was reduced with a focus on the Niger Delta area (see Fig. 5a) and the flares were allocated according to the cloud data grid with a mesh size of 0.03°.

Geosci. Model Dev. Discuss., doi:10.5194/gmd-2016-110, 2016
Manuscript under review for journal Geosci. Model Dev.
Published: 1 August 2016

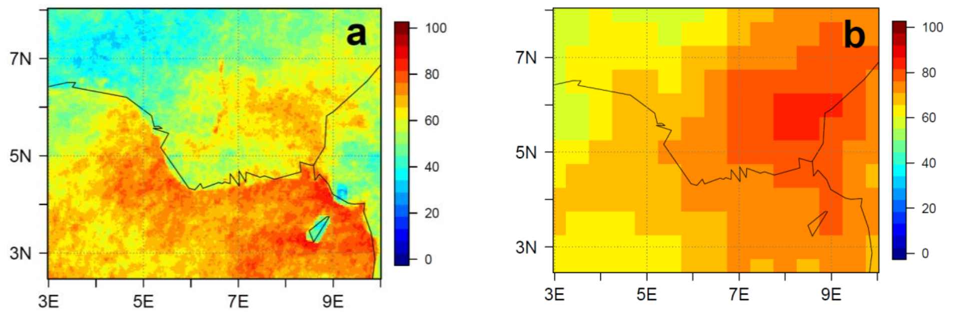

Fig.5. Fractional cloud cover (%) observed from (a) the geostationary MSG3 and (b) the sun-synchronous Aqua/AIRS, averaged over TP15 around the time of VNP observation (approx. 1 UTC).

Fig. 5a shows that the onshore flaring area for TP15 is in mean covered with clouds by 50-70%. For the offshore flaring area it is even higher with 70-90%. Therefore it is very likely that flares are frequently masked by clouds and therefore not detected by VNP. However, we suspect that the MSG3 cloud product underestimates (overestimates) the onshore (offshore) cloud cover when comparing with the findings of van der Linden et al. (2015). The high offshore coverage and the distinct land-water separation might be caused by overestimating low clouds in the presence of a warm and moist tropical ocean.

Fig. 5b shows a cloud climatology using Aqua/AIRS Nighttime data (Mirador, 2016). The Aqua/AIRS climatology shows higher cloud cover over land and no distinct separation between water and land surface. Both products identify the highest onshore cloud cover in the northeast of Port Harcourt (4.8°N, 7.0°E) and have similar values in the Nigerian offshore region (containing the offshore flares) of about 70-80%. The major difference in the climatologies appears onshore between 4.5°N and 6°N. This area includes the majority of the Nigerian onshore flares. Although it is not the aim of this study to identify the most reliable cloud climatology for SWA, it has to be considered that MSG3 likely underestimates the mean cloud cover over the Nigerian onshore flares up to 30%.

However, in the following the cloud climatology derived from MSG3 (Fig. 5a) is used since Aqua/AIRS cannot provide the full spatial coverage for every day (due to the sun-synchronous orbit of Aqua/AIRS).

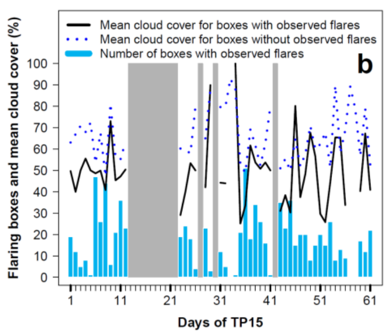

Fig.6. Number of boxes with detected flares per day (blue bars) and the mean fractional cloud cover for the boxes with (without) detected flares as black solid (blue dotted) line (using MSG3, compare Fig. 5a). For the calculation of the latter, the cloud cover of the non-active flare boxes within E_{clim} are averaged (compare Niger Delta area in Fig. 2b). The grey shaded areas are omitted due to lack of VNP observation.

Geosci. Model Dev. Discuss., doi:10.5194/gmd-2016-110, 2016
Manuscript under review for journal Geosci. Model Dev.
Published: 1 August 2016

Geoscientific Model Development Discussions

Fig. 6 shows the number of grid boxes with active flares per day in TP15 as blue bars. The grey areas indicate data gaps in VNP. E_{clim} includes 185 flare boxes according to the domain in Fig 5a. For TP15 not more than 51 flare boxes are detected at once. In average only 8% of the total flaring area is active at once. As expected the temporal evolution of the flare boxes and the cloud cover for these boxes (black solid line in Fig. 6) shows an anticorrelation. The highest number of flare boxes at day 36 is reached in a period of a comparatively low cloud cover. The mean cloud cover for the non-active flare boxes of E_{clim} (blue dotted line in Fig. 6), is in general higher than for the active flare boxes which implies that the cloud cover reduces the VNP detections. Fig. 6 also reveals that it is not suitable to use the strict cloud-free condition for the separation in Fig. 4B because nearly all of the boxes would be assigned to the dark blue cloud covered fraction and the resulting emissions would be nearly the same as E_{clim}.

However, it has to be considered that the light points of flares are extremely small-scale signals (1/5000 of the VNP pixel, Zhang et al. (2015)) and even for an almost completely closed cloud deck VNP detections are possible.

The climatology E_{clim} is the reference for this study. In addition we define E_{obs} which only considers the actually observed flares per day. E_{50} is defined as the combination of actually observed flares and cloud covered flares (see Fig. 4) with a cloud cover threshold of 50%. E_{75} (E_{90}) is equal to E_{50} but uses a cloud cover threshold of 75% (90%).

To emphasize the difference between the different emission estimates, Fig. 7 shows the daily emissions of CO_2 for TP15 as a spatial sum over the Niger Delta area (see Fig. 4a). In contrast to E_{clim} (black dashed line), E_{obs}, E_{50}, E_{75} and E_{90} (solid lines) have a temporal variation within TP15.

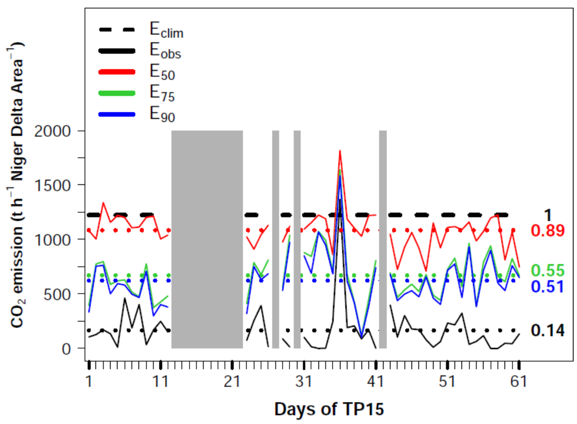

Fig.7. Daily CO_2 emissions (kg h^{-1}) within TP15 from flaring summed up over the Niger Delta area defined in Fig. 4a for the five emission estimates: E_{clim} (climatology, black dashed line), Eobs (VNP observations, black solid line), E_{50} (combination of VNP observations and the climatology for a cloud cover threshold of 50%, red solid line), E_{75} (as E_{50} but for a cloud cover threshold of 75%, green solid line), E_{90} (as E_{50} but for a cloud cover threshold of 90%, blue solid line). The dotted lines denote the spatiotemporal average of E_{obs}, E_{50}, E_{75} and E_{90}. The numbers on the right hand side show the ratios of the spatiotemporal averages E_{obs}, E_{50}, E_{75} and E_{90} towards E_{clim}. The grey shaded areas are omitted due to lack of VNP observation.

E_{clim} delivers a daily CO_2 emission of about 1250 t h^{-1} within the Niger Delta area. The pure daily VNP observations within E_{obs} (black solid line) show only 14% of E_{clim} emissions (numbers on left hand side of Fig. 7) on average (black dotted line). The emissions from VNP observations together with the climatology for the cloud threshold of 50% within E_{50} (red solid line) is closest to the climatology (89%

Geosci. Model Dev. Discuss., doi:10.5194/gmd-2016-110, 2016
Manuscript under review for journal Geosci. Model Dev.
Published: 1 August 2016

Geoscientific Model Development Discussions

of E_{clim}, red dotted line). The high overall cloud cover within the domain (compare with blue dotted line in Fig. 6) together with the relative low cloud cover threshold leads to the result, that nearly the complete climatology is used for E_{50} and therefore the difference to E_{clim} is small. The emissions from VNP observations together with the climatology for the cloud threshold of 75% and 90% within E_{75} and E_{90} (green and blue solid line) shows only small deviations but are significantly reduced in comparison to E_{clim} (55% and 51% of E_{clim}, green and blue dotted line). Day 36 of TP 15 shows highest emissions in E_{obs}, E_{50}, E_{75} and E_{90}, owing to the combination of low cloud cover and high flaring activity (compare with Fig. 6). Regarding the uncertainty in the cloud cover climatology (compare Fig. 5a and Fig. 5b), the emissions of E_{50}, E_{75} and E_{90} might be underestimated. The underestimation of the cloud cover in the onshore flaring area could lead to an unjustified increase in flare boxes below N_{th} and therefore to a reduced number of active flares per day.

These emission estimations contain different information. E_{clim} includes all flares of the domain despite cloud cover but can overestimate the emissions. E_{obs} shows the VNP reality, including a temporal development, but cannot consider the cloud-covered flares. E_{50}, E_{75} and E_{90} combine the flare location information of E_{clim} and the full temporal resolution of VNP in E_{obs} by using cloud observations. However this approach is based on the assumption that all cloud covered flare boxes are active, which is also linked to high uncertainty. Additionally E_{50}, E_{75} and E_{90} depend on the availability of a longer VNP observational dataset. The ratios of the spatiotemporal means of E_{obs}, E_{50}, E_{75} and E_{90} to the spatial mean of E_{clim} (as denoted by the numbers in Fig. 7) are used as correction factors (CF) for E_{clim} in the following (see Tab. 4). E_{clim} is taken as the reference (CF=1).

Tab.4. Emission estimations including information about flaring (daily observation and climatology) and cloud cover observation. The correction factors (CF) are derived for TP15 from a spatiotemporal emission mean in the Niger Delta area (2.5°N-8°N, 3°E-10°E) and refer to E_{clim}.

Name	Emission estimate	CF for E_{clim}
E_{clim}	Climatology (reference)	1
E_{obs}	Observed flares	0.14
E_{50}	Observed flares + climatology (N_{th}= 50%)	0.89
E_{75}	Observed flares + climatology (N_{th} = 75%)	0.55
E_{90}	Observed flares + climatology (N_{th} = 90%)	0.51

These CF are a simple method to include the information of E_{obs}, E_{50}, E_{75} and E_{90} into E_{clim} by multiplying E_{clim} with the corresponding correction factor. In this case the same 185 flare boxes of E_{clim} are used but with an emission strength reduced to the averaged conditions of E_{obs}, E_{50}, E_{75} and E_{90}. This approach is based on the assumption that the correction factor, deduced for the Niger Delta area, is valid for the whole domain specified in Section 3.1. This assumption seems to be justified since the Niger Delta area contains most of the gas flares in the domain.

3.3.2 Uncertainty due to IU14 input parameters

To assess the uncertainty which arises from the combustion efficiency η and the availability of combustion air δ, a sensitivity study has been carried out. The exact values for the SWA flares are unknown and very likely highly variable from one flare to another, depending on the flare type and operation. Fig. 8a shows the flare emissions averaged over SWA and TP15 for CO, CO_2, NO and NO_2. The parameters η and δ are varied referring to IU14. A complete combustion ($\eta = 1$) does not produce CO emissions since all carbon is transformed to CO_2 (not shown). With decreasing η and δ, the CO and CO_2 emissions increase. Concerning CO we assume the lower limit for $\eta = 0.9$ and

Geosci. Model Dev. Discuss., doi:10.5194/gmd-2016-110, 2016
Manuscript under review for journal Geosci. Model Dev.
Published: 1 August 2016

Geoscientific Model Development
Open Access
Discussions

$\delta = 1.3$ (left of Fig. 8a) and the upper limit for $\eta = 0.5$ and $\delta = 0.76$ (right of Fig. 8a). The values used for this study are located in the center of Fig. 8a. By taking the latter as reference, the lower (upper) limit leads to a decrease (increase) in CO emission of -63% (+210%). For CO_2 we derived an upper (lower) limit of +38% (-72%).

A higher combustion efficiency or a higher availability of combustion air allows an enhanced formation of NO. Therefore NO emissions increase (decrease) with decreasing η (δ). We assume the lower limit for $\eta = 0.9$ and $\delta = 0.95$ and the upper limit for $\eta = 0.5$ and $\delta = 1.30$. Taking again the central parameter set of Fig. 8a as reference, the lower (upper) limit leads to a decrease (increase) in NO emission of -77% (+441%).

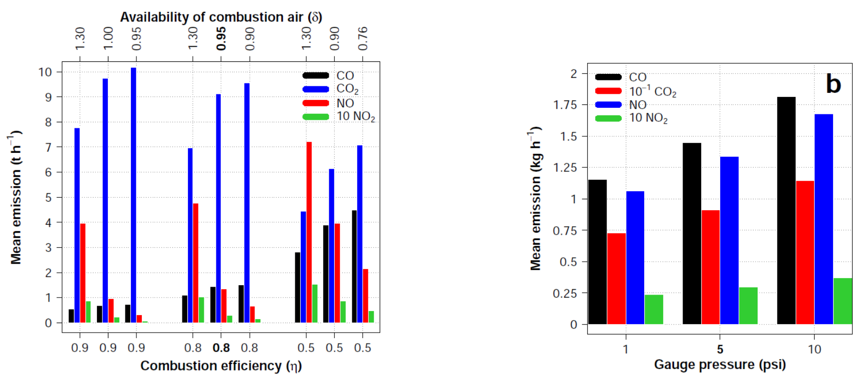

Fig.8. Flaring emissions (kg h^{-1}) spatiotemporally averaged over SWA and TP15 depending on (a) combustion efficiency η and availability of combustion air δ and (b) gauge pressure (psi) for the setup of η and δ which is used for this study (emphasized in bold). SO_2 is not shown because it does not depend on η or δ.

The emissions of NO_2 are comparatively low owing to the source temperature which is in general lower than the NO_2 formation threshold of 1600 K.

In addition, Fig. 8b shows the emissions depending on the gauge pressure for 1 (lower limit), 5 and 10 psi (upper limit) (7, 34 and 69 kPa respectively) for $\eta = 0.8$ and $\delta = 0.95$. Regarding 5 psi as the reference, the lower (upper) limit leads to a decrease (increase) in CO emissions of -21% (+26%).

Fig. 8 emphasizes that the technical conditions of flaring crucially influence the emission strength and that the emissions are more sensitive towards η and δ than towards the gauge pressure.

3.3.3 Uncertainty due to the fraction of radiated heat

To estimate the uncertainty in the fraction of radiated heat f (see Tab. 2), we have used the standard deviation of the literature values given in the appendix of Guigard et al. (2000) in addition to the mean value of $f = 0.27$. This leads to a domain of uncertainty for the value f of $(^{0.38}/_{0.16})$. Therefore the VNP observed radiant heat is multiplied with the factor $1/f$ of 3.7 $(^{6.2}/_{2.6})$.

3.3.4 Interannual variability

The differences in flaring between TP14 and TP15, indicated in Fig. 1 and Fig. 2, are quantified in this section according to the emissions of CO (Fig. 9a) and CO_2 (Fig. 9b). The boxplots include all flaring boxes for the two domains SWA (green) and the Niger Delta area (blue). The numbers above indicate the integrated emissions per hour and area in tons.

Geosci. Model Dev. Discuss., doi:10.5194/gmd-2016-110, 2016
Manuscript under review for journal Geosci. Model Dev.
Published: 1 August 2016

Geoscientific Model Development
Discussions

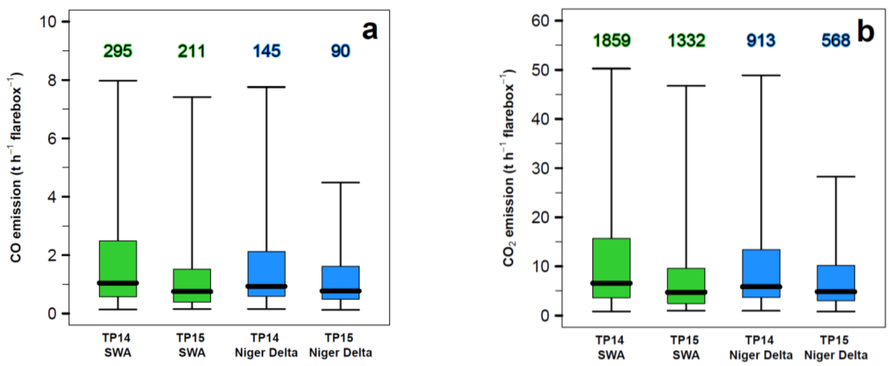

Fig.9. Flare box emissions of (a) CO and (b) CO_2 (E_{clim}, t h^{-1} $flarebox^{-1}$) for SWA (green) and the Niger Delta area (blue) for TP14 and TP15. The values above the boxplots indicate the emissions per hour, integrated over SWA (green) and the Niger Delta area (blue). The whiskers span the data range from the 0.025-quantile to the 0.975-quantile (95% of the data). Data outside of this range is not shown.

The emissions of CO_2 are 6.3 times higher than the CO emissions. For SWA the mean value of emissions is statistically significant lower for TP15 compared to TP14 (Wilcoxon-Mann-Whitney rank sum test with a significance level of 0.05). For the Niger Delta area the emission means show no significant difference. The significant different mean values for SWA emissions emphasize the relevance of using a flaring dataset which is up to date to reduce uncertainties arising from deviations in flare locations or flaring processes.

3.3.5 Uncertainty due to spatial variability in H_2S

Since hydrogen sulfide (H_2S) is the only sulfur source in the flared gas, it determines the emission of sulfur dioxide. The natural gas composition measurements from the ten flow stations given in Sonibare and Akeredolu (2004) contain only two stations with nonzero H_2S content. Therefore averaging over the ten stations (see Tab. 3) leads to a low H_2S content in the emission calculations. By using the highest concentration value of H_2S given in Sonibare and Akeredolu (2004) (see Tab. 3, H_2S concentration 0.03% instead of 0.005%), we try to estimate the upper limit of SO_2 emission, assuming that all flares are provided with this more sulfur containing gas. With this approach the spatiotemporal averaged SO_2 emissions increase from 0.6 to 4.9 kg h^{-1}. The maximum values in the flare boxes increase from 4.7 to 41.8 kg h^{-1}. These are rather low values.
This comparison reveals that among the flaring conditions also the natural gas composition plays an important role in estimating the flaring emissions reasonably. To rely on a single measurement dataset for a large flaring domain and without taking into account spatial variability is therefore problematic but has to be accepted owing to insufficient data.
This section has estimated the uncertainties in gas flaring due to cloud cover, parameters of IU14, the fraction of radiated heat, the temporal variability and the H_2S concentration in the natural gas. The uncertainty regarding the spatial variability of the total hydrocarbon fraction of the natural gas, which is estimated by the variations in the ten flow station measurements of Sonibare and Akeredolu (2004), is below 1%.
However, there are further assumptions or sources of uncertainty which cannot be quantified within this study: We assume that the natural gas composition, which is measured in one region, is valid for

Geosci. Model Dev. Discuss., doi:10.5194/gmd-2016-110, 2016
Manuscript under review for journal Geosci. Model Dev.
Published: 1 August 2016

Geoscientific Model Development Discussions

SWA entirely. The gas flares are taken as constant emission sources because VNP only provides one observation (overflight) per day. We cannot take into account the spatial variability of the flares concerning the IU14 parameters and the stack heights. And finally IU14 delivers no VOCs and black carbon.

4. Comparison with existing emission inventories

The following section places the estimated flaring emissions of this study in the context of existing emission inventories, by taking the focus on CO_2. A direct comparison with existing emission inventories is problematic due to different reference time periods, spatial domains, definitions of emission sectors and the limitation of chemical compounds. Tab. 5 summarizes the CO_2 emissions for different inventories regarding Nigeria or the Niger Delta area as denoted in Fig. 5a, the flaring hotspot of the research domain. The results of this study shows no flaring in the northern part of Nigeria and therefore flaring within the Niger Delta area can be seen as the total flaring area of the country. To derive annual emission values for the results of this study, it is assumed that the flaring emission conditions of TP14 and TP15 are representative for the whole year 2014 and 2015 respectively. Therefore the hourly emissions are integrated over 365 days.

Tab.5. Comparison between existing emission inventories for CO_2 (with a focus on gas flaring if available) and the results of this study for Nigeria or the Niger Delta area in teragram (Tg) per year. For TP14 and TP15 it is assumed that the two month observations represent the flaring conditions of the whole year 2014 and 2015 respectively. Therefore the emissions were integrated to yearly values. The values in brackets represent the upper and lower limit owing to the uncertainties estimated in Section 3. For the fraction of radiated f the mean value 0.27 and the lower (upper) boundary of 0.16 (0.38) are used, representing a further source of uncertainty. The products given in bold are directly related to flaring emissions.

Emission inventory	Time period	CO_2 emissions (Tg y^{-1})		
		$f = 0.16$	$f = 0.27$	$f = 0.38$
This study (E_{clim})	2014 (from TP14)	$13\ (^{19}/_{3})$	$8\ (^{12}/_{2})$	$6\ (^{8}/_{1})$
This study (E_{clim})	2015 (from TP15)	$8\ (^{12}/_{2})$	$5(^{7}/_{1})$	$4\ (^{5}/_{0})$
This study (E_{75})	2014 (from TP14)	$7\ (^{11}/_{2})$	$4\ (^{7}/_{1})$	$3\ (^{5}/_{0})$
This study (E_{75})	2015 (from TP15)	$5\ (^{7}/_{1})$	$3\ (^{4}/_{0})$	$2\ (^{3}/_{0})$
CDIAC (2015b)[1]	2011		27.47	
EIA (2015)[2]	2010; 2011; 2013		38.81; 41.39; 52.83	
Doumbia et al. (2014)[1]	2010		45	
EDGAR 4.2[3] (ECCAD, 2015)	2008		8.75	
EDGAR 4.2[4] (ECCAD, 2015)	2008		3.50	
EDGAR 4.3.2[5] (EDGAR, 2016)	2010; 2011; 2012		29.4, 28.8, 28.9	
EDGARv43FT2012[6] (EDGAR, 2014)	2014		93.87	

[1] from gas flaring, Nigeria
[2] from consumption and flaring of natural gas
[3] from refineries and transformation, Nigeria
[4] from refineries and transformation, Niger Delta area according to Fig. 5a
[5] from venting and flaring of oil and gas production, Nigeria
[6] emission totals of fossil fuel use and industrial processes (cement production, carbonate use of limestone and dolomite, non-energy use of fuels and other combustion). Excluded are: short-cycle biomass burning (such as agricultural waste burning) and large-scale biomass burning (such as forest fires), Nigeria

The CO_2 emission estimations of this study are given in Tab.5 together with an overall uncertainty range ($^{+38}/_{-72}$ %) including the uncertainty from the IU14 parameters η and δ ($^{+12}/_{-52}$ %) and the gauge pressure ($^{+26}/_{-21}$ %) and from spatial variability of total hydrocarbon. The latter uncertainty is small (below 1%) owing to the low variation in THC concentration in the measurements of Sonibare

Geosci. Model Dev. Discuss., doi:10.5194/gmd-2016-110, 2016
Manuscript under review for journal Geosci. Model Dev.
Published: 1 August 2016

Geoscientific Model Development Discussions
Open Access
EGU

and Akeredolu (2004). The uncertainty due to cloud cover is represented by E_{75}. Regarding the relatively large uncertainty there is no preference in one of the emission estimates E_{clim} and E_{obs}.
By assuming the uncertainty range of the fraction of radiated heat f between 0.16 and 0.38, the results of the study on hand show CO_2 emissions in the same order of magnitude as the Carbon Dioxide Information Analysis Center (CDIAC, 2015b), the Energy Information Administration (EIA, 2015) and the EDGARv.4.3.2 (EDGAR, 2016) database, with best results for $f = 0.16$ but with an overall tendency to underestimate the emissions. E_{clim} shows smaller deviations to the existing inventories than the cloud correction approach of E_{75}. A direct comparison is hindered by a time lag of 3-4 years and missing information about the uncertainties of CDIAC. The values of EIA are higher than those of CDIAC because EIA includes the consumption of natural gas in addition to gas flaring. Doumbia et al. (2014) combines Defense Meteorological Satellite Program (DMSP) observations of flaring with the emission factor method to derive flaring emissions. The results agree with EIA (2015) but are 64% higher than CDIAC (2015b).
The emission inventory EDGAR v4.2 (ECCAD, 2015) delivers 8.75 (3.50) Tg CO_2 y^{-1} for Nigeria (Niger Delta area) for the emission sector *refineries and transformation*, which is in good agreement with the results for the study on hand.
As a benchmark for the flaring CO_2, the total CO_2 emissions for Nigeria are given by EDGAR (2014), (fossil fuel use and industrial processes). Taking EDGAR (2014) as a reference for total CO_2 emissions of Nigeria, flaring emissions contributes by 9 $(^{13}/_{2})$% (2014; E_{clim} $f = 0.27$), 14 $(^{20}/_{3})$% (2014; E_{clim} $f = 0.16$), 9% (2008; ECCAD, 2015), 28% (2011; CDIAC, 2015b), 48% (2010; Doumbia et al., 2014) or 56% (2013; EIA, 2015). The large spread between the different inventories emphasizes the large uncertainty within the estimation of emissions from gas flaring.
A shortcoming of the PEGASOS_PBL-v2 (not shown) and the EDGAR v4.2 emission inventory is the lack of offshore flaring emissions in the Gulf of Guinea south of Nigeria. For CDIAC and EIA this cannot be verified since the data is only available as a single value per country.
The differences between the results of this study and the existing emission inventories might be caused by an underestimation of the flow rate by VNP and Eq. 1 or by an inconsistent definition of emission source sectors for the existing inventories. E_{clim}, E_{75}, Doumbia et al. (2014) and CDIAC (2015b) focus on gas flaring, whereas other products also include natural gas consumption and emissions from refineries and transformation which also can include non-flaring emissions within and outside the areas indicated as flaring area by the satellite imagery. In addition, the existing inventories do not provide current values (time lag of 2 to 6 years) and therefore not consider the emission reduction indicated by Fig. 9.

5. Discussion and conclusions

The gas flaring emission estimating method of Ismail and Umukoro (2014) (IU14) has been combined with the remote sensing flare location determination of the VIIRS Nightfire Prerun V2.1 Flares only (VNP) (VIIRS, 2015) for a new flaring emission parameterization. The parameterization combines equations of incomplete combustion with the gas flow rate derived from remote sensing parameters instead of using emission factors and delivers emissions of the chemical compounds CO, CO_2, NO and NO_2.
Within this study the parameterization was applied to southern West Africa (SWA) including Nigeria as the second biggest flaring country. Two two-month flaring observation datasets for June-July 2014 and 2015 were used to create a flaring climatology for both time periods. In this climatology all detected flares emit with their mean activity.

Geosci. Model Dev. Discuss., doi:10.5194/gmd-2016-110, 2016
Manuscript under review for journal Geosci. Model Dev.
Published: 1 August 2016

Geoscientific Model Development Discussions

The uncertainties owing to missed flare observations by cloud cover, parameterization parameters, interannual variability and the natural gas compositions were assessed. It can be shown that the highest uncertainties arise from the definition of the fraction of radiated heat f and the IU14 parameters. By using remote sensing cloud cover observations, a correction factor for the flaring climatological emission was derived which reduces the mean emissions about 50%. However, owing to the large uncertainty ranges, no significant difference between the climatological inventory and the cloud corrected inventory can be stated. Comparing the emissions of 2014 and 2015, a reduction in the flaring area, density of active flares and a significant reduction in SWA emissions about 30% can be observed, which underlines the need for more recent emission inventories.

The uncertainty due to the natural gas composition is compound dependent. The spatial variation in total hydrocarbon is negligible but the availability of hydrogen sulfide, which exclusively determines the amount of emitted SO_2, cause large uncertainty By taking the combustion efficiency to derive the fraction of unburned natural gas, the amount of emitted VOCs might be estimated in addition to the species of the study on hand but would also be linked to high uncertainties concerning the VOC speciation. The uncertainty in VOC emission is increased drastically by natural gas which is vented directly into the atmosphere instead of being flared, since the venting cannot be detected by VNP.

With a focus on Nigeria, the CO_2 emission estimates of this study were compared with existing inventories. For the climatology, CO_2 emissions of 8 $(^{12}/_{2})$ Tg y^{-1} for 2014 and 5 $(^{7}/_{1})$ Tg y^{-1} for 2015 were derived. EDGAR v4.2 for the year 2008 shows the same order of magnitude when limiting to emissions from refineries and transformation. CDIAC (Carbon Dioxide Information Analysis Center) is in the same order of magnitude as the results of this study. Doumbia et al. (2014) and EIA (Energy Information Administration) show emissions which are 2.4 and 2.8 times higher than the results of this study. The deviations might be caused by uncertainties in the flow rate derived by VNP radiant heat, which can be assessed only rudimentary via the parameter of the fraction of radiated heat. Additionally, the usage of emission factors in the existing inventories which did not take into account the spatiotemporal variability of flaring, inconsistent emission sector definitions or the time lag of the emission inventories of 2-5 years can lead to deviations. The positive trend in Nigerian gas flaring CO_2 emissions derived by EIA from 38.81 to 52.83 Tg y^{-1} between 2010 and 2013 contradicts the findings of Doumbia et al. (2014) and this study, which generally show a decrease in emissions from 1994 to 2010 and from 2014 to 2015, respectively. Based on the sensitivity study, which reveals high uncertainties of the flaring emission, we conclude that there is no preference in the choice of one of the emission estimates presented in this study. Therefore we recommend the use of the climatological approach when using the R package.

Despite the generally large uncertainties in the estimation of emissions from gas flaring, this method allows a flexible creation of flaring emission datasets for various applications (e.g. as emission inventory for atmospheric models). It combines observations with physical based background concerning the combustion. The use of current data makes it possible to consider present trends in gas flaring. Even the creation of near real-time datasets with a time lag of one day is possible. The emissions are merged on grid predefined by the user and depending on the availability of VNP data, the temporal resolution can be selected from single days to years.

An improvement of this parameterization can be achieved by an extension of the IU14 method to black carbon and VOCs and an inclusion of spatial resolved measurements of the natural gas composition in combination with information of the gas flaring processes from the oil producing industry.

Geosci. Model Dev. Discuss., doi:10.5194/gmd-2016-110, 2016
Manuscript under review for journal Geosci. Model Dev.
Published: 1 August 2016

Geoscientific Model Development Discussions

Acknowledgments

The research leading to these results has received funding from the European Union 7th Framework Programme (FP7/2007-2013) under Grant Agreement no. 603502 (EU project DACCIWA: Dynamics-aerosol-chemistry-cloud interactions in West Africa).

We are grateful to Godsgift Ezaina Umukoro (Department of Mechanical Engineering, University of Ibadan, Nigeria) for the kind support during the implementation of their combustion reaction theory into our parameterization. We also thank the Earth Observation Group (EOG) of NOAA for providing the *VIIRS Nightfire Flares Only product*.

Code and/or data availability

This publication includes a package of well documented R scripts which is free available for research purposes and enables the reader to create their own gas flaring emission datasets. It includes exemplarily the preprocessing for June-July 2015 with a focus on southern West Africa. You get access to the code via zenodo.org (DOI: 10.5281/zenodo.50938).

References

API, 2007: **Pressure-relieving and Depressuring Systems**, ANSI/API STANDARD 521 FIFTH EDITION, JANUARY 2007, ISO 23251 (Identical), Petroleum and natural gas industries – Pressure-relieving and depressuring systems, American Petroleum Institute, Section 7.3.2.4: Design details h), 127

Bader, A., Baukal, C. E., Bussman, W. Zink, J., 2011: **Selecting the proper flare systems**, American Institute of Chemical Engineers (AIChE), http://people.clarkson.edu/wwilcox/Design/FlareSel.pdf, accessed: October 2, 2014

CDIAC, 2015a: **Global CO2 Emissions from Fossil-Fuel Burning, Cement Manufacture, and gas Flaring: 1751-2008**, Carbon Dioxide Information Analysis Center (CDIAC), http://cdiac.ornl.gov/ftp/ndp030/global.1751_2008.ems, accessed: December 6, 2015

CDIAC, 2015b: **National CO2 Emissions from Fossil-Fuel Burning, Cement Manufacture, and gas Flaring: 1751-2011**, Carbon Dioxide Information Analysis Center (CDIAC), Fossil-Fuel CO_2 Emissions by Nation, http://cdiac.ornl.gov/ftp/ndp030/nation.1751_2011.ems, accessed: December 3, 2015

CM SAF, 2015: **Operational Products: CFC – Fractional cloud cover instantaneous data** (MSG disk, CM SAF definition), Version 350; https://wui.cmsaf.eu/safira/action/viewPeriodEntry?id=11495_14063_15657_15672_16574_19152_20532_21207, accessed: November 25, 2015

Doumbia, T., Granier, L., Liousse, C., Granier, C., Rosset, R., Oda, T., Fen Chi, H., 2014: **Analysis of fifty year Gas flaring Emissions from oil/gas companies in Africa**, AGU Fall Meeting 2014, Dec 2014, San Francisco, United States. A13E-3217

Dung, E. J., Bombom, L. S., Agusomu, T. D., 2008: **The effects of gas flaring on crops in the Niger Delta, Nigeria**, GeoJournal, Vol., 73, 297-305

Ekpoh, I. J., Obia, A. E., 2010: **The role of gas flaring in the rapid corrosion of zinc roofs in the Niger Delta Region of Nigeria**, Environmentalist, Vol. 30, 347-352

ECCAD, 2015: **Emissions of atmospheric compounds & compilation of ancillary data (ECCAD)**, http://eccad.sedoo.fr/eccad_extract_interface/JSF/page_critere.jsf, accessed: December 4, 2015

EDGAR, 2016: **Global Emissions EDGAR v4.3.2**, European Commission, Joint Research Centre (JRC)/PBL Netherlands Environmental Assessment Agency. Emission Database for Global Atmospheric Research (EDGAR), release version 4.3.2. http://edgar.jrc.ec.europe.eu

EDGAR, 2014: **Global Emissions EDGAR v4.3 FT2012**, European Commission, Joint Research Centre (JRC)/PBL Netherlands Environmental Assessment Agency. Emission Database for Global Atmospheric Research (EDGAR), release version 4.3. http://edgar.jrc.ec.europe.eu, 2015 forthcoming, http://edgar.jrc.ec.europa.eu/overview.php?v=CO2ts1990-2014, accessed: December 3, 2015

EIA, 2015: **CO2 from the Consumption and Flaring of Natural Gas**, International Energy Statistics, U.S. Energy Information Administration (EIA), http://www.eia.gov/cfapps/ipdbproject/iedindex3.cfm?tid=90&pid=3&aid=8&cid=&syid=2010&eyid=2013&unit=MMTCD, accessed: December 3, 2015

Elvidge, C. D., Zhizhin, M., Hsu, F.-C., Baugh, K. E., 2013: **VIIRS Nightfire: Satellite Pyrometry at Night**, Remote Sens., Vol. 5, 4423-4449

Elvidge, C. D., Ziskin, D., Baugh, K. E., Tuttle, B. T., Gosh, T., Pack, D. W., Erwin, E. H., Zhizhin, M., 2009: **A fifteen year record of global natural gas flaring derived from satellite data**, Energies, Vol. 2, 595-622

Elvidge, C. D., Baugh K. E., Kihn, E. A., Kroehl, H. W., Davis, E. R., 1997: **Mapping city lights with nighttime data from the DMSP operation linescan system**, Photogrammetric Engineering & Remote Sensing, Vol. 63, No. 6, 727-744

EPA, 1985: **Evaluation of the efficiency of industrial flares: Flare head design and gas composition**, Research and Development, United States Environmental Protection Agency (EPA), EPA-600/2-85-106, Tab. 2-6

Google Earth, 2014: Image 2014 DigitalGlobe, http://www.earth.google.com

Guigard, S. E., Kindzierski, W. B., Harper, N., 2000: **Heat Radiation from Flares**. Report prepared for Science and Technology Branch, Alberta Environment, ISBN 0-7785-1188-X, Edmonton, Alberta.

Ismail, O. S., Umukoro, G. E., 2014: **Modelling combustion reactions for gas flaring and its resulting emissions**, Journal of King Saud University – Engineering Sciences, article in press, doi:10.1016/j.jksues.2014.02.003

Johnson, M. R., Devillers, R. W., Thomson, K. A., 2011: **Quantitative Field Measurements of Soot Emission from Large Gas Flare using Sky-LOSA**, Environ. Sci. Technol., Vol. 45, 345-350

Knippertz, P., Evans, M. J., Field, P. R., Fink, A. H., Liousse, C., Marsham, J. H., 2015: **The possible role of local air pollution in climate change in West Africa**, Nature Climate Change, Vol. 5, 815-822

Mirador, 2016: AIRS/Aqua Level 2 Standard physical retrieval (AIRS+AMSU), Total cloud fraction (CldFrcTot), mirador.gsfc.nasa.gov/cgi/bin/mirador/presentNavigation.pl?tree=project& Project=AIRS&data, accessed: April 18, 2016

NASA, 2016: http://npp.gsfc.nasa.gov/viirs.html, accessed: January 5, 2016

Nwankwo, C. N., Ogagarue, D., O., 2011: **Effects of gas flaring on surface and ground waters in Delta State Nigeria**, Journal of Geology and Mining Research, Vol. 3, 131-136

Nwaugo, V. O., Onyeagba, R. A., Nwahcukwu, N. C., 2006: **Effect of gas flaring on soil microbial spectrum in parts of Niger Delta area of southern Nigeria**, African Journal of Biotechnology, Vol. 5, 1824-1826

Osuji, L. C., Avwiri, G. O., 2005: **Flared Gas and Other Pollutants Associated with Air quality in industrial Areas of Nigeria: An Overview**, Chemistry & Biodiversity, Vol. 2, 1277-1289

R Core Team, 2013: **R: A Language and Environment for Statistical Computing**, R Foundation for Statistical Computing, Vienna, Austria, http://www.R-project.org/

Sonibare, J. A., Akeredolu, F. A., 2004: **A theoretical prediction of non-methane gaseous emissions from natural gas combustion**, Energy Policy, Vol. 32, 1653-1665

Strosher, M. T., 2000: **Characterization of Emissions from Diffuse Flare Systems**, Journal of the Air & Waste Management Association, 50:10, 1723-1733

Strosher, M. T., 1996; **Investigations of flare gas emissions in Alberta**, Final Report to: Environment Canada, Conservation and protection, the Alberta Energy and Utilities Board, and the Canadian Association of Petroleum Producers; Environmental Technologies, Alberta Research Council, Calgary, Alberta

TA-Luft, 1986: **Technische Anleitung zur Reinhaltung der Luft 1986.** Heider-Verlag, 5060 Bergisch Gladbach 2, Anhang C: Ausbreitungsrechnung, Eq. 2.1, 127-139

van der Linden, R., Fink, A. H., Redl, R., 2015: **Satellite-based climatology of low-level continental clouds in southern West Africa during the summer monsoon season**, Journal of Geophysical Research: Atmospheres, Vol. 120, 1186-1201

VIIRS, 2015: http://ngdc.noaa.gov/eog/viirs/download_viirs_flares_only.html, accessed: November 6, 2015

Vogel, B., Vogel, H., Bäumer, D., Bangert, M., Lundgren, K., Rinke, R., Stanelle, T., 2009: **The comprehensive model system COSMO-ART - Radiative impact of aerosol on the state of the atmosphere on the regional scale**, Atmos. Chem. Phys., 9, 8661-8680

World Bank, 2012: http://www.worldbank.org/content/dam/Worldbank/Programs/Top 20 gas flaring countries.pdf, accessed: December 5, 2015

Zhang, X., Scheving, B., Shoghli, B., Zygarlicke, C., Wocken, C., 2015: **Quantifying Gas Flaring CH_4 Consumption Using VIIRS**, Remote Sens., Vol. 7, 9529-9541